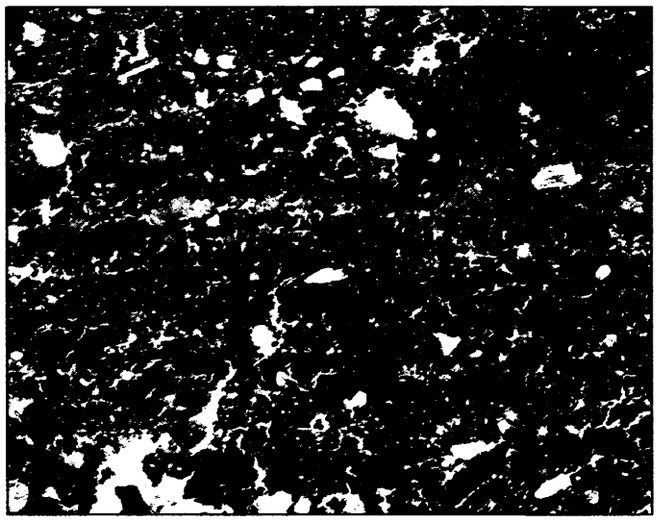

Fig. 3. Photomicrograph of Layer 10, illustrating the presence of massive sediments in the upper part and finely laminated, blackish organic matter (silts) in the lower part. The brighter orange-colored material is a secondarily precipitated phosphate, probably carbonated apatite. Regardless of whether the dark-colored organic matter in the lower part is a result of actual burning or aging, it is certainly not in its primary context but is water laid. The image was made with plane-polarized light; the width of the photograph is about 3 mm.

and of in situ hearth features that there is no direct evidence for in situ burning in Layers 4 and 10. Most of the fine-grained sediments in the site were water laid, and even if ash remains could be recognized, it would be difficult to demonstrate where they were produced. The co-occurrence of burned black bones and quartzite artifacts in the same layers is only suggestive of a cultural association, and hence of the use of fire by humans, but does not prove it. As most of the site has, however, already been excavated, it is not now possible to determine the locations of any campfires in Locality 1 at Zhoukoudian.

References and Notes

1. J. A. J. Gowlett, J. W. K. Harris, D. Walton, B. A. Wood, *Nature* **294**, 125 (1981).
2. M. Barbetti, *J. Hum. Evol.* **15**, 771 (1986).
3. C. K. Brain and A. Sillen, *Nature* **336**, 464 (1988).
4. S. R. James, *Curr. Anthropol.* **30**, 1 (1989).
5. K. Oakley, *Prehist. Soc.* **4**, 36 (1955).
6. S. Zhang, in *Palaeoanthropology and Palaeolithic Archaeology in the People's Republic of China*, W. U. Rukang and J. W. Olsen Eds. (Academic Press, London, 1985), pp. 147–186.
7. S. L. Guo *et al.*, *Nucl. Tracks Radiat. Meas.* **19**, 719 (1991).
8. R. Grün *et al.*, *Hum. Evol.* **32**, 83 (1997).
9. W. Pei and S. Zhang, *A Study of the Lithic Artifacts of Sinanthropus, Palaeontologica Sinica*, vol. 12 (Science Press, Beijing, 1985).
10. D. Black, T. De Chardin, C. C. Young, W. C. Pei, *Mem. Geol. Surv. China Ser. A* **11**, 1 (1933).
11. Z. Yang *et al.*, in *Multi-Disciplinary Study of the Peking Man Site at Zhoukoudian*, W. Rukang *et al.*, Eds. (Science Press, Beijing, 1985), pp. 1–85.
12. L. R. Binford and C. K. Ho, *Curr. Anthropol.* **26**, 413 (1985).
13. L. R. Binford and N. M. Stone, *ibid.* **27**, 453 (1986).
14. C. B. Stringer, *ibid.* **26**, 655 (1985).
15. Z. Liu, *Quat. Res.* **23**, 139 (1985).
16. ———, *Geoarchaeology* **3**, 103 (1988).
17. R. Shahack-Gross, O. Bar-Yosef, S. Weiner, *J. Archaeol. Sci.* **24**, 439 (1997).
18. G. S. Humphreys, P. A. Hunt, R. Buchanan, *Aust. J. Soil Res.* **25**, 115 (1987).
19. S. Schiegl, S. Lev-Yadun, O. Bar-Yosef, A. El-Goresy, S. Weiner, *Israel J. Earth Sci.* **43**, 267 (1994).
20. S. Schiegl, P. Goldberg, O. Bar-Yosef, S. Weiner, *J. Archaeol. Sci.* **23**, 763 (1996).
21. A 0.5-g aliquot of the sediment was treated with a mixture of 3N HCl and 3N HNO_3 for 30 min at 100°C. The acid was removed by centrifugation (at 6000 rpm for 2 min), and the pellet was washed twice with water. The pellet was resuspended in 5 ml of sodium polytungstate solution (density 2.4), thoroughly dispersed by sonication, and then centrifuged as above. The supernatant was removed and diluted with 1 ml of water, vortexed, and recentrifuged. This was repeated until no mineral remained in the supernatant.
22. P. Bullock, N. Federoff, A. Jongerius, G. J. Stoops, T. Tursina, *Handbook For Soil Thin Section Description* (Waine Research Publishers, Wolverhampton, UK, 1985).
23. M. A. Courty, P. Goldberg, R. Macphail, *Soils and Micromorphology in Archaeology* (Cambridge Univ. Press, Cambridge, 1989).
24. In Mousterian sediments in Kebara and Hayonim caves, Israel, the overall proportions of relatively large burned bones (based on their black color) are 5.2% (*25*) and 13% (M. C. Stiner, unpublished data), respectively. In Grotta dei Moscerini and Grotta di Sant' Agostini, Italy, the proportions vary between 1 and 7%, except for two levels in which they are 32 and 52% (*26*). At the Henderson site, New Mexico, the proportion of bison and ungulate burned bones is 8.6%, whereas for rodent bones it is 1.5% (*25*).
25. J. D. Speth, unpublished data.
26. M. C. Stiner, S. L. Kuhn, S. Weiner, O. Bar-Yosef, *J. Archaeol. Sci.* **22**, 223 (1995).

27. We thank L. Estroff for her help. This project was supported by grants from the Israel Science Foundation to S.W., from the L. S. B. Leakey Foundation to P.G., from the American School of Prehistoric Research (Peabody Museum, Harvard) to O.B.-Y., and from the Natural Science Foundation of China to Q.X.

5 March 1998; accepted 18 May 1998

Design of a 20–Amino Acid, Three-Stranded β-Sheet Protein

Tanja Kortemme,*† Marina Ramírez-Alvarado,*† Luis Serrano

A 20-residue protein (named Betanova) forming a monomeric, three-stranded, antiparallel β sheet was designed using a structural backbone template and an iterative hierarchical approach. Structural and physicochemical characterization show that the β-sheet conformation is stabilized by specific tertiary interactions and that the protein exhibits a cooperative two-state folding-unfolding transition, which is a hallmark of natural proteins. The Betanova molecule constitutes a tractable model system to aid in the understanding of β-sheet formation, including β-sheet aggregation and amyloid fibril formation.

Despite the importance of β-sheet structures as regular secondary structure elements in proteins, the principles underlying their formation and stability are not well understood. A major obstacle to the study of β-sheet structures is the tendency of isolated β-sheet secondary structure elements to aggregate. Formation of amyloid fibrils mediated by the interaction of β strands is thought to be a crucial event in the progression of a wide variety of pathological disorders, ranging from Alzheimer's disease to spongiform encephalopathies (*1*). Until now, the scarce information available on the determinants of β-sheet stability has been obtained from systematic mutagenesis experiments (*2, 3*) and, more recently, through the study of de novo–designed simple β-hairpin peptides (two antiparallel β strands connected by a β turn or a short loop) (*4, 5*). This lack of knowledge is attested to by the failure so far to design an all–β-sheet protein that is soluble, monomeric, and amenable to structural characterization in atomic detail (*6*), although a nuclear magnetic resonance (NMR) model of β-sheet formation coupled to oligomerization has been reported (*7*). This contrasts with the growing number of successfully designed α-helical proteins (*8*) and α/β proteins (*9, 10*), as well as with work directed toward the modification of sequences of β proteins to cause them to adopt α-helical structure (*11*). Consequently, the design of an all–β-sheet protein is a substantial challenge and could provide insight into the pathological processes mentioned above.

A key feature for the successful design of model proteins is to make them simpler than

European Molecular Biology Laboratory (EMBL), Meyerhofstrasse 1, Heidelberg D-69117, Germany.

*These authors contributed equally to this work.
†To whom correspondence should be addressed. E-mail: Kortemme@EMBL-Heidelberg.DE (T.K.) and Ramirez@EMBL-Heidelberg.DE (M.R.-A.).

their natural counterparts, yet able to attain a unique conformation in aqueous solution (*12*). Our goal has therefore been the design of a small, soluble, monomeric, model β-sheet protein containing only natural amino acids, which would fold in the absence of disulfide bonds or metal binding sites. We selected a three-stranded antiparallel β sheet composed of four residues per strand and two-residue β turns as our backbone framework (Fig. 1A), which is a minimal unit retaining all the characteristics of larger β-sheet proteins. We performed selection and optimization of a sequence compatible with our target backbone structure, considering experimental information on β-hairpin stability (*13*), amino acid β-sheet propensities (*2, 3*), and statistical preferences for interstrand residue pairs (*14*), and evaluating combinations of side chain rotamers (side chain rotamer modeling). An iterative design and analysis procedure (Fig. 1B) (*15*) resulted in the successful design of a 20–amino acid three-stranded β sheet (named Betanova).

Our initial sequence was a longer version of a designed de novo β-hairpin peptide (*5*) that adopts a folded structure in equilibrium with random coil conformations (hairpin I). The hairpin structure was elongated by placement of a Lys^+-Glu^- pair at the outer edges of the previous model peptide (hairpin II), leading to an increase in the structured population from about 35% to about 45% (*16*). The hairpin II sequence was placed on the central (β strand 2) and COOH-terminal (β strand 3) β strands of our framework. For the NH_2-terminal β strand (β strand 1), we searched for the best sequence in terms of statistical analysis of the protein structure database and favorable van der Waals contacts, using rotamer modeling. The turn sequences were selected to be optimal for type I′ β turns in β hairpins (*17*). The resulting peptide (sheet I) was soluble and monomeric up to a concentration of 3 mM. NMR analysis showed evidence for structure only in the region corresponding to hairpin II.

In a new set of peptides (sheets II and III), some of the residues in β strand 1 were changed to modify the interstrand packing and to introduce an additional Asp^-/Glu^--Lys^+ ionic pair. We found that sheets II and III behaved similarly to sheet I. However, the designed sheet I sequence folded into the target structure upon addition of 40% 2,2,2-trifluoroethanol. This indicated that the lack of formation of a well-defined three-stranded β sheet in aqueous solution was not the result of side chain–side chain incompatibilities at the interface between the NH_2-terminal and central β strands. A likely explanation is that the amount of hydrophobic surface area buried by the four aliphatic side chains on β strands 1 and 2 is not sufficient to drive β-sheet formation. In contrast, the sequence corresponding to hairpin II buries a large hydrophobic surface area because of the favorable packing of a Tyr residue (β strand 3) with the side chains of Ile, Val (β strand 2), and Lys (β strand 3). These results prompted us to search for the possibility of introducing an aromatic residue into β strand 1 in order to create extensive contacts with residues on β strand 2. Exploring different rotamers for aromatic residues in β strand 1 showed that an aromatic side chain could pack favorably onto the surface of the β-sheet structure only in the absence of β-branched residues on β strand 2. A good example of this residue arrangement is found in WW domains (so termed because of the conservation of two tryptophane residues in this protein domain family) (*18, 19*). Considering this information and molecular modeling using the ICM (internal coordinates mechanics) package (*20*), we modified the sheet I sequence and termed this new sequence Betanova (Fig. 1).

The Betanova molecule (*21*) was soluble in water and monomeric up to a concentration of 2.6 mM, as determined by analytical ultracentrifugation, circular dichroism (CD), and NMR spectroscopy (*22*). The presence of characteristic long-range backbone-backbone and side chain–side chain nuclear Overhauser effects

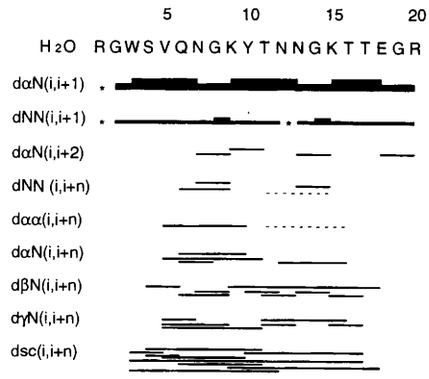

Fig. 2. Summary of NOE connectivities defining the β-sheet conformation of Betanova. The NOEs were taken from 130-ms NOESY spectra obtained at 273 and 280 K. Asterisks and dotted lines refer to NOEs that could not be detected because of signal overlap. The height of the bars for the sequential NOEs reflects their relative intensities. NOEs between side chains are grouped as "dsc."

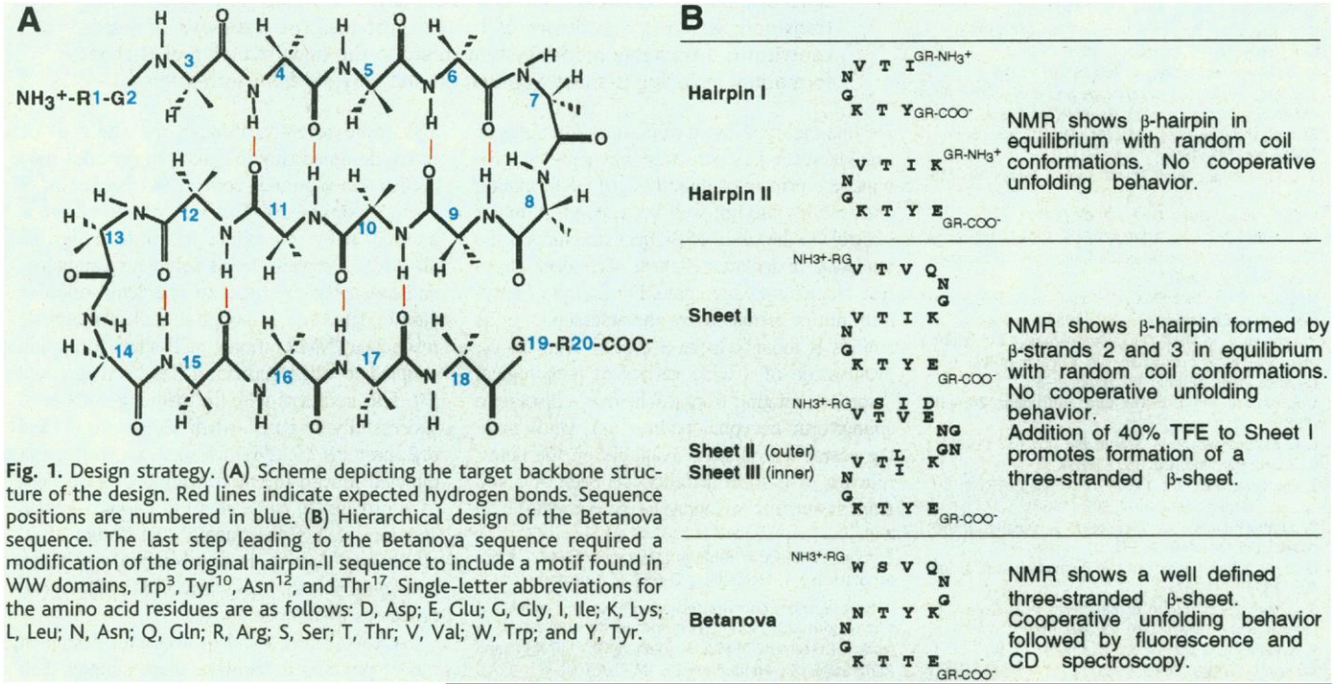

Fig. 1. Design strategy. (**A**) Scheme depicting the target backbone structure of the design. Red lines indicate expected hydrogen bonds. Sequence positions are numbered in blue. (**B**) Hierarchical design of the Betanova sequence. The last step leading to the Betanova sequence required a modification of the original hairpin-II sequence to include a motif found in WW domains, Trp^3, Tyr^{10}, Asn^{12}, and Thr^{17}. Single-letter abbreviations for the amino acid residues are as follows: D, Asp; E, Glu; G, Gly, I, Ile; K, Lys; L, Leu; N, Asn; Q, Gln; R, Arg; S, Ser; T, Thr; V, Val; W, Trp; and Y, Tyr.

(NOEs) (*23*) between residues in adjacent β strands and, more important, the NOEs between aromatic protons of Trp^3 and Cγ protons of Thr^{17} (Fig. 2) indicated the formation of the desired three-stranded β sheet. This was corroborated by the large $^3J_{NH\alpha}$ coupling constant values measured for β-strand residues, as well as by the conformational secondary chemical shift profiles of the $^{13}C\alpha$ and $^{13}C\beta$ carbon nuclei (*24*).

A hallmark of proteins with defined native conformation, when compared to partly folded proteins or peptides, is that the former exhibit cooperative folding/unfolding transitions. The denaturation process of Betanova was monitored by CD and fluorescence spectroscopy (Fig. 3) (*25*). Betanova displayed cooperative behavior both by thermal (Fig. 3A) and chemical (Fig. 3B) denaturation, with a broad transition as expected from its small size (2.3 kD). The experimentally determined dependence of free energy on denaturant concentration (the *m* value) was 0.4 kcal mol^{-1} M^{-1}. This value, which is indicative of the amount of surface area exposed upon unfolding, is in very good agreement with the expected values for the calculated total buried surface area (*26*). The free energy change at 278 K obtained from both thermal and chemical denaturation was similar (around −0.6 to −0.7 kcal mol^{-1}).

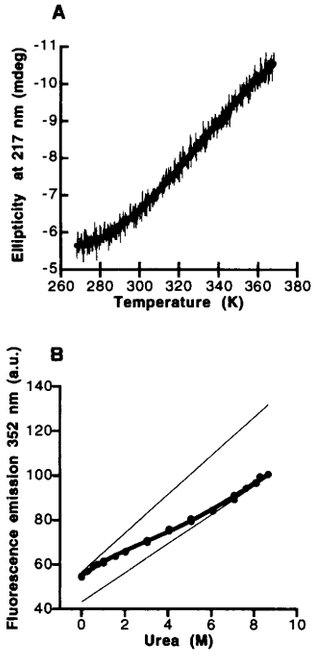

Fig. 3. (**A**) Thermal denaturation of Betanova monitored by CD at 217 nm. The curve represents the average of five independent measurements. The fit to the data to a two-state cooperative unfolding model is depicted as a continuous line. Applying a linear fit yields significant systematic deviations from the experimental data, thus supporting the conclusion of cooperativity. The observed decrease in ellipticity upon thermal denaturation results from the strong contribution of aromatic residues to the far-UV CD spectrum around 210 to 230 nm and has been observed in other all β-sheet proteins (*30*). (**B**) Chemical denaturation of Betanova monitored by fluorescence emission at 352 nm. The experimental points represent data from two independent experiments. The thick continuous line depicts fitting of the data. The initial and final baselines, shown as thin lines, are strongly dependent on urea concentration because of the presence of a partly exposed tryptophane residue.

We determined a three-dimensional model structure of Betanova compatible with the NOE and $^3J_{NH\alpha}$ coupling constant data (*27*). All 45 structures without NOE violations larger than 0.2 Å calculated with the dynamics algorithm for NMR applications (DYANA) exhibit the expected antiparallel, three-stranded β-sheet fold with two-residue turns located at the designed positions and the expected right-handed twist of the β sheet (*28*) (Fig. 4A). The first and last two residues appear to be disordered, as expected from the design, which includes terminal Arg residues for solubility and Gly residues as flexible linkers to the structured region as described previously (*5*). Comparison of the averaged minimized structure obtained from the NMR restraints with the target model shows a root-mean-square (rms) deviation of 1.11 Å for the backbone, demonstrating the success of our design (Fig. 4B). The packing of aromatic side chains in β sheets appears to contribute significantly to their stability, as well as to establish important conformational constraints for defining a single conformation (Fig. 4C).

It is remarkable that this designed β sheet has no real hydrophobic core (residues inaccessible to solvent), and although there is a hydrophobic cluster on one face of the β sheet, most of the residues involved in the packing also have polar groups (Fig. 4C). The absence of a hydrophobic core most likely induces a certain flexibility in the β sheet while still allowing defined tertiary interactions.

The simplicity of Betanova, together with the fact that it retains all the structural properties of β-sheet proteins, makes it an optimum model to use in refining existing molecular dynamics protocols, as well as to test recent theoretical approaches to protein folding (*29*). Recently developed computational methods for protein design have shown that it is possible to explore and evaluate all possible amino acid sequences for a given protein framework (*10*). This raises the question of how many sequences can adopt the same stable fold. Betanova constitutes a suitable system for exploring the sequence space experimentally.

The design of a β-sheet protein using information derived from de novo design and from structural stabilizing motifs demonstrates that we are starting to understand the principles behind β-sheet formation. The small size of the designed protein is critical for rationalizing the rules governing protein

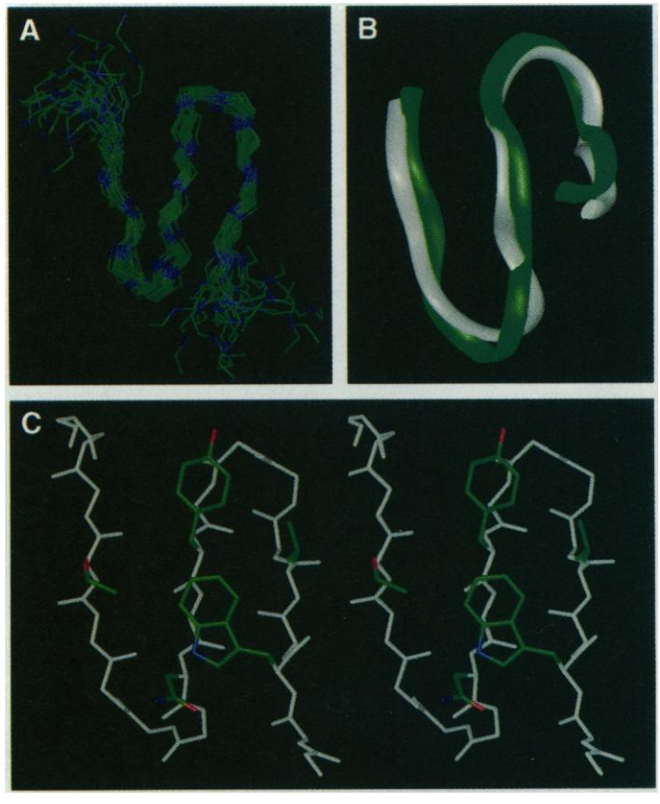

Fig. 4. (**A**) Backbone traces of the best 20 structures obtained from NMR restraints. Carbon atoms are depicted in green; nitrogen atoms in blue. (**B**) Superposition of the minimized average NMR structure of Betanova (gray) and the target backbone framework (green), in ribbon representation, used for sequence selection. (**C**) Minimized average NMR structure of Betanova, showing the hydrophobic cluster involving the side chains of Trp^3, Val^5, Tyr^{10}, Asn^{12}, and Thr^{17}. Tyr^{10} is interacting with Val^5, thus allowing the tryptophane side chain to rotate inward and pack onto the β sheet, as expected from the rotamer modeling.

architecture and folding, as well as for the development of suitable scaffolds for introducing different functionalities. This knowledge may help to elucidate the mechanisms leading to β-sheet aggregation.

Note added in proof: Schenck and Gellman reported the characterization of a three-stranded β sheet using D-proline in the turn and an unnatural amino acid in one of the strands (*31*).

References and Notes

1. J. W. Kelly, *Structure* **5**, 595 (1997); D. R. Booth *et al.*, *Nature* **385**, 787 (1997).
2. D. L. Minor Jr. and P. S. Kim, *Nature* **367**, 660 (1994); *ibid.* **371**, 264 (1994).
3. C. K. Smith and L. Regan, *Science* **270**, 980 (1995).
4. E. de Alba, M. A. Jiménez, M. Rico, J. L. Nieto, *Folding Des.* **1**, 133 (1996).
5. M. Ramírez-Alvarado, F. J. Blanco, L. Serrano, *Nature Struct. Biol.* **3**, 604 (1996).
6. A. Pessi, *et al.*, *Nature* **362**, 367 (1993); T. P. Quinn, N. B. Tweedy, R. W. Williams, J. S. Richardson, D. C. Richardson, *Proc. Natl. Acad. Sci. U.S.A.* **91**, 8747 (1994); Y. Yan and B. W. Erickson, *Protein Sci.* **3**, 1069 (1994).
7. E. Ilyina, V. Roongta, K. Mayo, *Biochemistry* **36**, 5245 (1997).
8. L. Regan and W. F. DeGrado, *Science* **241**, 976 (1988); M. H. Hecht, J. S. Richardson, D. C. Richardson, R. C. Ogden, *ibid.* **249**, 884 (1990); S. Kamtekar, J. M. Schiffer, H. Xiong, J. M. Babik, M. H. Hecht, *ibid.* **262**, 1680 (1993); J. W. Bryson *et al.*, *ibid.* **270**, 935 (1995); C. E. Schafmeister, S. L. LaPorte, L. J. W. Miercke, R. M. Stroud, *Nature Struct. Biol.* **4**, 1039 (1997).
9. K. Goraj, A. Renard, J. A. Martial, *Protein Eng.* **3**, 259 (1990); M. D. Struthers, R. P. Cheng, B. Imperiali, *Science* **271**, 342 (1996).
10. B. I. Dahiyat and S. L. Mayo, *Science* **278**, 82 (1997); B. I. Dahiyat, C. A. Sarisky, S. L. Mayo, *J. Mol. Biol.* **273**, 789 (1997).
11. D. T. Jones *et al.*, *Proteins Struct. Funct. Genet.* **24**, 502 (1996); S. Dalal, S. Balasubramanian, L. Regan, *Nature Struct. Biol.* **4**, 548 (1997).
12. W. F. DeGrado, Z. R. Wasserman, J. D. Lear, *Science* **243**, 622 (1989).
13. F. J. Blanco, M. Ramírez-Alvarado, L. Serrano, *Curr. Opin. Struct. Biol.* **8**, 107 (1998).
14. M. A. Wouters and P. M. G. Curmi, *Proteins Struct. Funct. Genet.* **22**, 119 (1995).
15. All sequence selection steps for β-sheet design were based on the use of two peptide backbone templates corresponding to antiparallel β sheets: fragment 57–72 of glyceraldehyde-3-phosphate dehydrogenase from *Bacillus stearothermophilus* {Protein Data Bank accession code 1gd1 [T. Skarzynoski, P. C. E. Moody, A. J. Wonacott, *J. Mol. Biol.* **193**, 171 (1987)]} and the WW domain of the mouse formin-binding protein, fragment 8–30 (*20*). The WW domain fragment contained loops between the β strands, which were changed to ideal, two-residue, type I′ β turns to yield a three-stranded antiparallel β sheet with four residues per strand, connected by two-residue β turns for both backbone templates. The different sequences were evaluated by the lowest van der Waals energies calculated by the ICM package (*20*). The template structures were prepared for sequence evaluation by a regularization procedure included in the ICM package that undergoes a rotational positioning of methyl groups, an iterative optimization of geometry and energy of the whole structure, and an adjustment of polar hydrogen positions.
16. M. Ramírez-Alvarado, F. J. Blanco, L. Serrano, unpublished data.
17. M. Ramírez-Alvarado, F. J. Blanco, H. Niemann, L. Serrano, *J. Mol. Biol.* **273**, 898 (1997).
18. M. J. Macías *et al.*, *Nature* **382**, 646 (1996).
19. M. J. Macías and H. Oschkinat, personal communication.
20. R. A. Abagyan, M. M. Totrov, D. N. Kuznetsov, *J. Comp. Chem.* **15**, 488 (1994).
21. The Betanova polypeptide was synthesized by the laboratory of R. Frank at the Center for Molecular Biology, Heidelberg University (ZmBH), using standard 9-fluorenyl-methoxycarbonyl chemistry. Purification to >95% was achieved by reversed-phase high-performance liquid chromatography. The molecular mass of the peptide was confirmed by mass spectroscopy.
22. Sedimentation equilibrium studies were performed at 278 K at a peptide concentration of 1.3 mM in aqueous solution (pH 5.0), using a Beckman XL-A ultracentrifuge equipped with a An-50 Ti rotor at a speed of 50,000 rpm. Fitting of the equilibrium radial concentration distribution to an ideal single-component model using a partial specific volume of 0.6825×10^{-3} m^3 kg^{-1}, calculated from the amino acid sequence, resulted in a molecular mass of 2259 daltons, which is in excellent agreement with the expected molecular mass for a monomer of 2257 daltons. The monomeric state of Betanova was additionally confirmed by the concentration independence of the far-ultraviolet (UV) CD spectra between 5 μM and 1 mM in 5 mM sodium acetate (pH 5.0) and of the NMR line widths and chemical shift values at peptide concentrations between 20 μM and 2.6 mM, in 90% (v/v) ^1H_2O/10% ^2H_2O (pH 5.0).
23. NMR measurements were performed at temperatures of 273, 278, and 280 K in 90% (v/v) ^1H_2O/10% ^2H_2O (pH 5.0) at a peptide concentration of 2.6 mM, or in 99.8% ^2H_2O (pH 5.0) (uncorrected for deuterium isotope effects) at a peptide concentration of 2.2 mM. Spectra were acquired on Bruker DRX-500 or DRX-600 spectrometers, operating at 500.13 and 600.13 MHz, respectively. Samples contained sodium 3-trimethylsilyl (2,2,3,3-$^2H_4$) propionate as an internal reference. double-quantum filter correlated spectroscopy (DQFCOSY) [U. Piantini, O. W. Sørensen, R. R. Ernst, *J. Am. Chem. Soc.* **104**, 6800 (1982)], NOE spectroscopy (NOESY) [J. Jeener, B. H. Meier, P. Bachmann, R. R. Ernst, *J. Chem. Phys.* **71**, 4546 (1979); S. Macura and R. R. Ernst, *Mol. Phys.* **41**, 95 (1980); mixing time (τ_m) = 100, 130, and 200 ms], and rotating frame overhauser effect spectroscopy (ROESY) [A. A. Bothner-By, R. L. Stephens, J. M. Lee, C. D. Warren, R. W. Jeanloz, *J. Am. Chem. Soc.* **106**, 811 (1984); τ_m = 100, 130, and 200 ms] spectra were acquired for resonance assignment using standard procedures [K. Wüthrich, *NMR of Proteins and Nucleic Acids* (Wiley, New York, 1986)]. NOESY and ROESY spectra were jointly analyzed to discard artifactual NOEs as those arising from spin diffusion. Total correlated spectroscopy (TOCSY) [A. Bax and D. G. Davies, *J. Magn. Reson.* **65**, 355 (1985); τ_m = 80 ms] spectra were acquired using the standard MLEV-17 spin lock sequence. Water suppression was achieved by selective presaturation during the relaxation delay (1.2 s) or field-gradient pulses [M. Piotto, V. Saudek, V. Sklenar, *J. Biomol. NMR* **2**, 661 (1992); V. Sklenar, M. Piotto, R. Leppik, V. Saudek, *J. Magn. Reson.* **A102**, 241 (1993)]. The spin-spin coupling constants $^3J_{HN\alpha}$ were measured from 2D TOCSY and NOESY spectra using the method of Stonehouse and Keeler as implemented in the program MEDEA [J. Stonehouse and J. Keeler, *J. Magn. Reson.* **A112**, 43 (1995)]. $^{13}C\alpha$ and $^{13}C\beta$ chemical shifts were obtained from natural abundance ^{13}C heteronuclear multiple quantum coherence (HMQC) spectra [A. Bax, R. H. Griffey, B. L. Hawkins, *ibid.* **55**, 301 (1983)].
24. T. Kortemme, M. Ramírez-Alvarado, L. Serrano, data not shown. The conformational shifts of the $^{13}C\alpha$ and $^{13}C\beta$ nuclei are available as supplementary material at *Science* Online at www.sciencemag.org/feature/data/980831.shl.
25. CD measurements were recorded on a JASCO-710 spectropolarimeter equipped with a Peltier-type temperature control system. Thermal denaturation was monitored at 217 nm in a 2-mm stoppered cuvette, with a temperature slope of 50°C hour^{-1}, at a peptide concentration of 100 μM in 5 mm sodium acetate (pH 5.0) containing 10% (v/v) glycerol. The glycerol was present to allow measurements at temperatures down to 268 K. Measurements between 273 and 368 K gave identical traces in the presence and absence of glycerol. Reversibility was demonstrated by cooling the solution and repeating the thermal denaturation, resulting in a profile identical to the initial measurement. Van't Hoff analysis of the data yielded values of the enthalpy change at 278 K ($\Delta H_{(278K)}$ = 3.3 kcal mol^{-1}), of the entropy change at 278 K ($\Delta S_{(278K)}$ = 0.01 kcal mol^{-1} K^{-1}), and of the free energy change at 278 K ($\Delta G_{(278K)}$ = −0.6 kcal mol^{-1}), indicating the presence of 80 to 90% folded structure under these conditions. The energy values have to be considered approximate because of the difficulty in defining the upper baseline of the transition. The value for the heat capacity at constant pressure (ΔC_p) used in the analysis was estimated from the change in accessible polar and nonpolar surface area upon unfolding, according to (*26*) or as described by K. P. Murphy and E. Freire [*Adv. Prot. Chem.* **43**, 313 (1992)]. In both cases, the value for ΔC_p was around 0.14 kcal mol^{-1} K^{-1}. Chemical denaturation by urea was followed using fluorescence spectroscopy. Urea concentrations were determined refractometrically. Fluorescence emission at 352 nm (excitation, 290 nm) was measured at 278 K at a peptide concentration of 6 μM using an Aminco Bowman Series 2 luminescence spectrometer. The denaturation profile was fitted to $F = \{F_F + A \times [\text{urea}] + ((F_U + B \times [\text{urea}]) \times \exp((-\Delta G_{H_2O} + (m[\text{urea}]))/RT))\}/\{1 + \exp((-\Delta G_{H_2O} + (m[\text{urea}]))/RT)\}$, where A and B are the slopes of the urea dependence of the fluorescence of the folded and unfolded states, respectively. F, F_F, and F_U are the observed fluorescence values at a particular urea concentration and the fluorescence of the folded state and that of the unfolded state, respectively. ΔG_{H_2O} is the free energy of unfolding in the absence of urea, and m is the dependence of ΔG_{H_2O} on denaturant concentration. Fitting yielded an m value of 0.4 kcal mol^{-1} M^{-1} and a ΔG_{H_2O} of −0.7 kcal mol^{-1}. The obtained m value is in excellent agreement with the one expected (0.44 kcal mol^{-1} M^{-1}) for a protein of this size, using the empirical correlation described in (*26*). However, the experimental values of m and ΔG_{H_2O} have to be taken with caution because of the small change in fluorescence between folded and unfolded states and the large error in the estimation of the slopes of the urea dependence of the fluorescence of the folded and unfolded states, arising from the solvent exposure of the Trp side chain.
26. J. K. Myers, C. N. Pace, J. M. Scholtz, *Protein Sci.* **4**, 2138 (1995).
27. Cross-peak intensities were obtained from 130-ms NOESY spectra collected at 273 and 280 K in 90% (v/v) ^1H_2O/10% ^2H_2O (pH 5.0) or 99.8% ^2H_2O (pH 5.0). Each NOE was classified as strong, medium, weak, or very weak by visual inspection of the contour levels or intensity integration of the cross-peaks in NOESY spectra and was assigned to upper-limit distance restraints as follows: strong (2.5 Å), medium (3.5 Å), weak (5.0 Å), and very weak (5.5 Å). Dihedral restraints were derived from the $^3J_{HN\alpha}$ coupling constants. With a set of 40 sequential, 48 nonsequential, and 11 dihedral restraints, a family of 45 structures without NOE violations larger than 0.2 Å were generated using DYANA [P. Güntert, C. Mumenthaler, K. Wüthrich, *J. Mol. Biol.* **273**, 283 (1997)]. The rms deviation from the average minimized structure in the well-ordered region of residues 3–18 was 0.96 Å for the backbone atoms and 1.93 Å for all heavy atoms.
28. C. Chothia, *J. Mol. Biol.* **75**, 295 (1973).
29. T. Lazaridis and M. Karplus, *Science* **278**, 1928 (1997).
30. J. Prieto, M. Wilmans, M. A. Jiménez, M. Rico, L. Serrano, *J. Mol. Biol.* **268**, 760 (1997).
31. H. L. Schenck and S. H. Gellman, *J. Am. Chem. Soc.* **120**, 4869 (1998).

32. We thank M. J. Macías and H. Oschkinat for communicating results before publication; H. van der Zandt for help with the sedimentation equilibrium measurements; T. Creighton and M. Saraste for critical reading of the manuscript; M. Sattler for discussions concerning NMR experiments; and M. Petukhov, E. Lacroix, and J. Martínez for helpful discussions. This work was partly supported by a European Union Biotechnology grant (BIO4-CT97-2086).

18 February 1998; accepted 20 May 1998